

Semileptonic B Decays at $BABAR$ *

Urs Langenegger[†]

Physikalisches Institut, Philosophenweg 12, D-69120 Heidelberg, Germany[‡]

ursl@physi.uni-heidelberg.de

We present results on semileptonic B decays obtained with the $BABAR$ detector. The large data set accumulated at the PEP-II asymmetric-energy B -Factory allows a new measurement technique, where the hadronic decay of one B meson is fully reconstructed and the semileptonic decay of the recoiling B meson is studied. Traditional analysis techniques of inclusive and exclusive B decays complement this approach with very high statistics data samples. These measurements play an important role in the tests of the description of CP violation in the Standard Model: The determinations of the Cabibbo-Kobayashi-Maskawa matrix elements $|V_{cb}|$ and $|V_{ub}|$ provide constraints on the unitarity of the CKM triangle. Furthermore, the experimental measurement of parameters of Heavy Quark Effective Theory test the consistency of the theoretical description of semileptonic B decays.

Keywords: Semileptonic B Decays; $BABAR$; CKM Physics

PACS Nos.: 13.20.He Decays of beauty mesons and 12.15.Nh Determination of Kobayashi-Maskawa matrix elements

1. Introduction

The principal motivation for the study of flavor physics is a comprehensive test of the Standard Model description of CP violation. Semileptonic B decays allow for a direct determination of $|V_{cb}|$ and $|V_{ub}|$, two elements of the Cabibbo-Kobayashi-Maskawa (CKM) quark mixing matrix. In the unitarity triangle, the precision of $|V_{cb}|$ affects constraints derived from kaon decays and the overall normalization, while the uncertainty in $|V_{ub}|$ dominates the error of the length of the side opposite the angle β . As this angle can be measured very cleanly in time-dependent CP asymmetries, the errors of $|V_{ub}|$ must be model independent, well understood, and small before any discrepancies between sides and angles could be interpreted as new physics. This is not yet the case: the error in $|V_{ub}|$ is larger than 10% and dominated by theoretical uncertainties.^{1,2}

In the theoretical description of semileptonic B decays, the large mass of the b quark plays a central role by implying special symmetries and a hard scale.³ This is formulated by Heavy Quark Effective Theory⁴ (HQET) for exclusive decays and an

*Originally based on an invited seminar first given at CERN, with updated results.

[†]Work supported in part by Department of Energy contract DE-AC03-76SF00515.

[‡]Address before October 2003: Stanford Linear Accelerator Center, Stanford, CA 94309, USA

Operator Product Expansion⁵ (OPE) for inclusive decays. Both provide systematic expansions of the (differential) decay rate in terms of Λ_{QCD}/m_b and $\alpha_s(m_b)$. Here in calculable quantities are parametrized in terms of expectation values of hadronic matrix elements, which can be related to the shape (moments) of inclusive decay spectra. The large rate of Cabibbo-favored decays $\bar{B} \rightarrow X_c \ell \bar{\nu}$ allows for precise measurements of the relevant distributions and the determination of HQET parameters. This provides precision determinations of $|V_{cb}|$ and stringent quantitative tests of the consistency of the theory.

The situation is different for Cabibbo-suppressed $\bar{B} \rightarrow X_u \ell \bar{\nu}$ decays: the large rate for $\bar{B} \rightarrow X_c \ell \bar{\nu}$ decays constitutes a background that is about 50 times larger, overlapping in most of the phase space. Experimentally, selection criteria are applied to reduce this background, but can lead to problems in the theoretical description.

The experimental approach to semileptonic decays can be separated into two classes: Exclusive decays reconstruct one signal decay mode, *e.g.*, $\bar{B}^0 \rightarrow D^{*+} \ell^- \bar{\nu}$. Even though the neutrino cannot be measured directly, this approach is relatively straightforward. The inclusive analysis of semileptonic decays is often based on the measurement of the charged lepton alone, or by combining hadronic final states X without disentangling specific resonances.

2. The *BABAR* Detector

The measurements presented here are based on data collected by the *BABAR* detector⁶ at the PEP-II asymmetric energy e^+e^- collider near the $\Upsilon(4S)$ resonance. Most of the analyses use an integrated luminosity of about 80 fb^{-1} , corresponding to about 89 million $B\bar{B}$ pairs. The $\Upsilon(4S)$ resonance is just above threshold for the decay into a pair of B mesons (either B^+B^- or $B^0\bar{B}^0$), without any other fragmentation particles. Furthermore, the two B mesons have a low and known momentum of $p_B^* = 320 \text{ MeV}/c$ in the center-of-mass system (CMS)^a, leading to spherically symmetric decays. This is different for $q\bar{q}$ continuum processes (where $q = u, d, s, c$), which exhibit a more jet-like structure. This is exploited with event shape variables and neural networks.

At a CMS energy of $\sqrt{s} = 10.58 \text{ GeV}$, the $\Upsilon(4S)$ production cross-section amounts to about 1.1 nb . This corresponds to a rate of about $10 B\bar{B}$ pairs/sec at an instantaneous luminosity of $10^{34} \text{ cm}^{-2} \text{ s}^{-1}$. Given the total hadronic continuum cross section of ca. 3.5 nb , the resulting signal to background ratio is much higher than at hadronic colliders. The background from continuum processes is determined in dedicated “off-peak” runs, where the CMS energy is lowered to $\sqrt{s} = 10.54 \text{ GeV}$.

A five-layer silicon vertex tracker provides precision vertexing and low-momentum charged particle tracking, down to transverse momenta $p_\perp \sim 50 \text{ MeV}$. This is especially important for the reconstruction of $D^{*+} \rightarrow D^0 \pi_s^+$ decays, where the “slow” pion π_s has very low energies. A 40-layer driftchamber surrounds the ver-

^aAll variables measured in the CMS frame, *e.g.*, p_B^* , are marked with a star.

tex detector and complements the momentum measurement. In addition, the dE/dx measurements are used in the identification of low-momentum electrons. The DIRC provides detection of internally reflected Cherenkov light used in charged hadron identification. The electromagnetic CsI(Tl) crystal calorimeter is the most important detector for electron identification (by means of the ratio E/p of the deposited energy E and the momentum p). In addition, its measurements of neutral particles is crucial for the inclusive determination of the invariant mass m_X in $\bar{B} \rightarrow X\ell\bar{\nu}$ decays. The detector is surrounded by a superconducting coil (providing a magnetic field of 1.5 T) and its instrumented flux return, used in the identification of muons.

The boosted CMS at *BABAR* leads to a limited coverage of about 85% of the solid angle in the CMS. This is a notable disadvantage for the reconstruction of neutrinos from the missing momentum, as about 1 GeV of energy is missed per event (on average).

3. Recoil Physics

The very large luminosity at the *BABAR* detector allows for a new paradigm for the systematic study of semileptonic B decays. Traditionally⁷ events are selected (“tagged”) by a high-momentum lepton, signaling the semileptonic decay of one of the B mesons and thereby reducing $q\bar{q}$ continuum events.

At *BABAR*, an alternative event tagging technique has been developed: the hadronic decay of one B meson (B_{reco}) is fully reconstructed and the semileptonic decay of the other B meson is identified by the presence of an electron or muon. This approach results in a low overall event selection efficiency, but allows for the determination of the momentum, charge, and flavor of the B mesons. It also provides a direct determination of the hadronic final state in $\bar{B} \rightarrow X\ell\bar{\nu}$ decays, as all particles in the recoil of the B_{reco} candidate originate from the other B meson decaying semileptonically. This method also offers a promising way to study semileptonic $\bar{B} \rightarrow X\tau\bar{\nu}_\tau$ decays.

A very large sample of B mesons is reconstructed by selecting hadronic decays^b $B_{reco} \rightarrow \bar{D}Y^+, \bar{D}^*Y^+$, where the hadronic system Y^+ consists of $n_1\pi^\pm n_2K^\pm n_3K_S^0 n_4\pi^0$, with $n_1 + n_2 \leq 5$, $n_3 \leq 2$, and $n_4 \leq 2$. The kinematic consistency of B_{reco} candidates is checked with the beam energy-substituted mass $m_{ES} = \sqrt{s/4 - \vec{p}_B^2}$ and the energy difference $\Delta E = E_B - \sqrt{s}/2$, where \sqrt{s} is the total energy and (E_B, \vec{p}_B) denotes the momentum four-vector of the B_{reco} candidate in the CMS. For each of the reconstructed B decay modes, the purity \mathcal{P} is estimated as the signal fraction in events with $m_{ES} > 5.27 \text{ GeV}/c^2$ (see Fig. 1). A priori, the purity of this sample is low, but improves substantially in conjunction with the requirement of a high momentum lepton in the recoil. By combining more than 300 modes, at least one B_{reco} candidate is reconstructed in 0.3% (0.5%) of the $B^0\bar{B}^0$ (B^+B^-) events. In events with more than one reconstructed B_{reco} candidate,

^bCharge conjugation is implied throughout the text.

we select the decay mode with the highest purity.

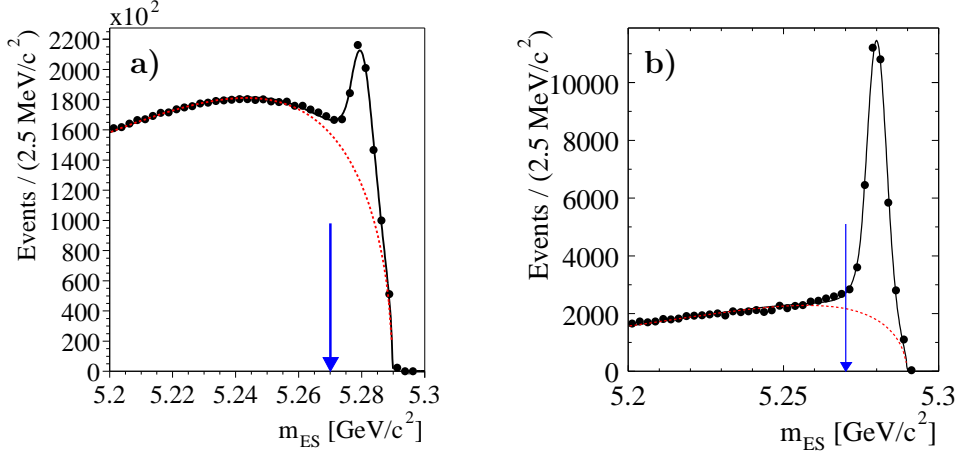


Fig. 1. The m_{ES} distributions for fully reconstructed hadronic B decays used in the event selection for the study of semileptonic B decays. a) With no requirement on the rest of the event, the purity amounts to 26%. b) With a $p^* > 1 \text{ GeV}/c$ lepton, the purity improves to 67%. The arrows indicate the minimum m_{ES} requirement used in the selection of signal events.

4. $\bar{B}^0 \rightarrow D^{*+} \ell^- \bar{\nu}$

While the decay mode $\bar{B}^0 \rightarrow D^{*+} \ell^- \bar{\nu}$ has a large branching fraction, the measurements so far are not very consistent—recent results range from $(4.59 \pm 0.46)\%$ to $(6.09 \pm 0.44)\%$. The very large luminosity at *BABAR* opens new possibilities for the precision determination of this decay.

The theoretical description of $B \rightarrow D^{(*)} \ell \bar{\nu}$ decays in terms of HQET⁴ predicts the differential decay rate schematically as

$$\frac{d\Gamma(\bar{B} \rightarrow D^{(*)} \ell \bar{\nu})}{dw} = \mathcal{K} \cdot |V_{cb}|^2 \cdot \begin{cases} (w^2 - 1)^{1/2} \cdot \mathcal{F}_*^2(w) \\ (w^2 - 1)^{3/2} \cdot \mathcal{F}^2(w) \end{cases} \quad (1)$$

where $w \equiv v_B \cdot v_{D^*} = E_{D^*}/m_{D^*}$, $\mathcal{F}_{(*)}(w)$ is the formfactor describing the hadronization into a $D^{(*)}$ meson, and \mathcal{K} is a known and constant factor. The Lorentz factor w of the c -quark in the b -quark rest-frame takes values between $w = 1$ (“zero-recoil” situation: the c -quark is at rest) and $w = 1.5$ (c -quark and $\ell \bar{\nu}$ leaving back-to-back). In the limit of $m_Q \rightarrow \infty$ the formfactors $\mathcal{F}_{(*)}(w)$ are equal to the Isgur-Wise function.⁸ Heavy quark symmetry provides the normalization constraint $\mathcal{F}_{(*)}(1) = 1$. At zero-recoil, the light degrees of freedom (the spectator quark, the sea quarks and gluons) are not sensitive to the flavor change of the heavy quark. Because of the finite mass of the b and c quarks, small corrections need to be computed—this is done with phenomenological models or (currently quenched) lattice QCD calculations.

The experimental approach consists in the measurement of the differential rate $d\Gamma/dw$ as a function of w , and the extrapolation of the data to $w = 1$ to obtain $\mathcal{F}(1)|V_{cb}|$. This measurement is preferentially done with $\bar{B} \rightarrow D^*\ell\bar{\nu}$ instead of $\bar{B} \rightarrow D\ell\bar{\nu}$ decays: The decay rate is kinematically suppressed at $w = 1$ for both decays, but less so for $\bar{B} \rightarrow D^*\ell\bar{\nu}$. By virtue of Luke's theorem,⁹ there are no corrections at order $1/m_b$ or $1/m_c$ for $\bar{B} \rightarrow D^*\ell\bar{\nu}$, but they are present for $\bar{B} \rightarrow D\ell\bar{\nu}$ and thus increase the theoretical errors in this case. The background from high-mass X_c states constitutes a difficult experimental systematic problem. The decay $\bar{B} \rightarrow D\ell\bar{\nu}$ is even more affected by this, as the decay $\bar{B} \rightarrow D^*\ell\bar{\nu}$ here is a background process with a branching fraction that is about two times larger.

The event selection in this analysis¹⁰ starts from a charged lepton (e or μ) with momentum $p^* > 1.2$ GeV and a reconstructed $D^{*+} \rightarrow D^0\pi_s$ decay, where the D^0 is reconstructed in four modes: $D^0 \rightarrow K^-\pi^+$, $K_S^0\pi^+\pi^-$, $K^-\pi^+\pi^-\pi^+$, $K^-\pi^+\pi^0$. The mass difference $\delta m = m_{D^0\pi_s} - m_{D^0}$ is used for the selection of D^{*+} candidates and the determination of the combinatorial background. Given the very large data sample, it is possible to study and constrain most of the backgrounds directly in data: We study the uncorrelated background (where the lepton and D^{*+} originate from different B mesons) in control samples based on the opening angle between the D^{*+} and the lepton (signal decays tend to be back-to-back). Continuum background is reduced with event shape variables, the remaining component is subtracted with off-resonance data. The determination of the most dangerous background from high-mass X_c states in data is described in the next section. The only component taken from Monte Carlo (MC) simulations is the correlated background, where $B \rightarrow D^{*+}X$, $X \rightarrow Y\ell$.

At the $\Upsilon(4S)$, the known momentum magnitude of the B mesons provides sensitivity to the missing mass in the signal decay $\bar{B}^0 \rightarrow D^{*+}\ell^-\bar{\nu}$ from the observed particles D^{*+} and ℓ . Assuming that the only unmeasured particle is a massless neutrino, the angle between the momenta of the B^0 and the combined $D^*\ell$ is

$$\cos\theta_{B,D^*\ell} = \frac{2E_BE_{D^*\ell} - m_B^2 - m_{D^*\ell}^2}{2|\vec{p}_B||\vec{p}_{D^*\ell}|}. \quad (2)$$

This quantity will lie in the physical range for a signal decay (modulo resolution effects; signal events are required to have $|\cos\theta_{B,D^*\ell}| < 1.2$). Decays with additional missing particles will lead to a tail at low values, illustrated in Fig. 2 for $\bar{B}^0 \rightarrow D^{*+}e^-\bar{\nu}$ decays, where the background from $D^{*+}\ell\bar{\nu}$ exhibits a long tail. This is also visible for signal decays, due to missed photons from bremsstrahlung. For the extrapolation to zero-recoil, the decay rate must be measured differentially in $w = (m_{B^0}^2 + m_{D^*}^2 - q^2)/(2m_{B^0}m_{D^*})$, where $q^2 = (p_{B^0} - p_{D^*})^2$. The direction of the B^0 momentum is obtained from eq. 2 up to an azimuthal ambiguity about the direction of the $D^*\ell$ pair: an unbiased estimator of w with a resolution of $\sigma(w) \sim 0.02$ is calculated from the average of the two solutions corresponding to minimal and maximal angle between the B^0 and D^{*+} mesons.

The signal yield as a function of w is determined with a fit based on a quadratic

formfactor parametrization¹¹ (see Fig. 2). Based on ca. 57000 signal events, we obtain $|V_{cb}| = (37.27 \pm 0.26_{stat} \pm 1.43_{syst}^{+1.48}_{-1.23_{theo}}) \times 10^{-3}$. The dominant systematic errors of this result are due to tracking and vertexing (but not the slow pion efficiency), D^0 branching fractions and B lifetimes, and $f_{00} \equiv \mathcal{B}(\mathcal{T}(4S) \rightarrow B^0 \bar{B}^0)$. The theoretical error in the lattice calculation for $F_*(1) = 0.913^{+0.030}_{-0.035}$ is balanced among statistical, fitting, matching, spacing, mass, and quenching components.¹²

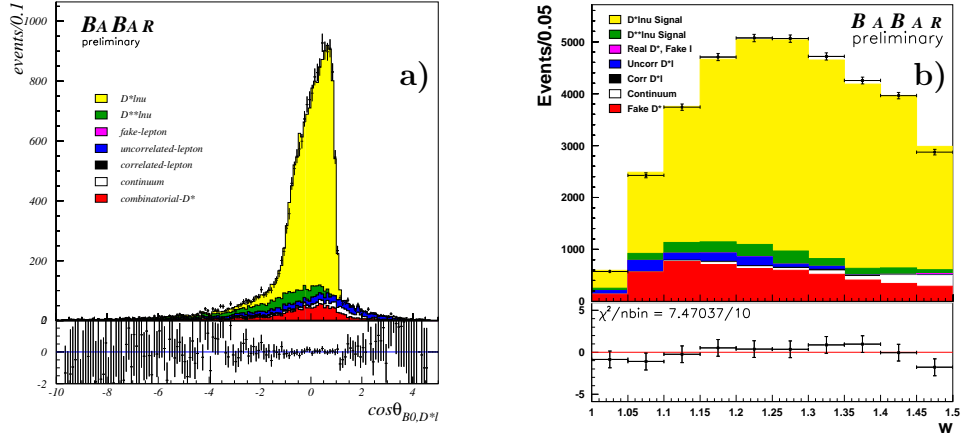


Fig. 2. a) Distribution of $\cos \theta_{B^0, D^* \ell}$ for the decay $\bar{B}^0 \rightarrow D^{*+} e^- \bar{\nu}_e, D^0 \rightarrow K^- \pi^+$, where the points show the data and the filled histograms represent the MC components. The MC normalization is determined in a fit. The bottom plot shows the fractional deviation of the data from the fit result. b) Comparison of the w distribution for $\bar{B}^0 \rightarrow D^{*+} e^- \bar{\nu}_e$ in data and the result of the fit. The fit residuals are shown in the bottom plot.

The branching fraction $\mathcal{B}(\bar{B} \rightarrow D^* \ell \bar{\nu}) = (4.68 \pm 0.03_{stat} \pm 0.29_{syst})\%$ is determined by integrating the differential w distribution (cf. eq. 1) thus reducing the uncertainties from formfactor parametrizations. These results are somewhat lower than other measurements (especially the recent one by CLEO¹³). As all measurements are systematically limited, a complementary approach, *e.g.*, in the recoil of a fully reconstructed B candidate, will be a very interesting result addressing the largest errors. The theoretical uncertainties associated with the extrapolation to $w = 1$ might be much reduced with a sample of the order of 10^6 signal decays.

5. Inclusive Cabibbo-favored Decays

In the description of exclusive $\bar{B}^0 \rightarrow D^{*+} \ell^- \bar{\nu}$ decays, the HQET relies on both m_b and m_c being large. For inclusive decays, this requirement can be relaxed to $m_b \gg \Lambda_{QCD}$, expressing the separation between the very short time scale relevant for the weak b -quark decay and the long time scale for the hadronization of the hadronic remnant. The OPE⁵ can be combined with HQET to calculate, *e.g.*,

the total semileptonic width Γ_{sl} in a power series in Λ_{QCD}/m_b and a perturbative expansion in $\alpha_s(m_b)$. Incalculable quantities are parametrized in terms of nonperturbative hadronic matrix elements. At lowest order, the OPE expression reduces to the parton model. There are no power corrections at order Λ_{QCD}/m_b in the total rate. The leading corrections are parametrized with

- $\bar{\Lambda} = m_B - m_b + (\lambda_1 + 3\lambda_2)/2m_b$, the energy of the light degrees of freedom. To first order, $\bar{\Lambda}$ is the mass difference of the b quark and the B meson.
- λ_1 is the negative kinetic energy squared of the b quark in the B meson.
- λ_2 describes the chromomagnetic coupling of the b quark spin to the light degrees of freedom.

Note that these parameters are scheme and order dependent. At higher orders many more parameters ($\rho_1, \rho_2, \mathcal{T}_1, \dots, \mathcal{T}_4$, etc.) enter, none of which are currently well known. They constitute a large fraction of the theoretical errors.

These parameters are not restricted to the description of the total semileptonic rate, they also appear in the calculation of differential semileptonic B decay spectra and in other B decays: $\bar{\Lambda}$ can be related to the mean photon energy of the decay $b \rightarrow s\gamma$, and λ_2 can be determined from the mass difference of B^* and B mesons.

The parameters can be related to the shape of decay spectra in semileptonic $\bar{B} \rightarrow X\ell\bar{\nu}$ decays, such as the lepton energy spectrum E_ℓ or the invariant hadronic mass spectrum m_X . The inclusive description of semileptonic $\bar{B} \rightarrow X\ell\bar{\nu}$ decays does not distinguish between specific hadronic final states X , *e.g.*, the D and D^* mesons. To compare, *e.g.*, the theoretical expectation for the m_X distribution with the measured spectrum, it is therefore necessary to resort to observables smearing the differential spectrum. A simple and sensitive possibility is given by moments of various order. As different moments have different dependencies on the parameters, a simultaneous fit to several moments provides for an experimental determination of the nonperturbative parameters. The large branching fraction for $\bar{B} \rightarrow X\ell\bar{\nu}$ allows for a very precise determination of these parameters. We can therefore shift a large fraction of the theoretical errors into (smaller) experimental errors, which are more amenable to a proper statistical interpretation. This is essential for a quantitative understanding of the errors of the extracted CKM parameters.

5.1. Inclusive Semileptonic Branching Fraction

The model-independent measurement of the total inclusive semileptonic branching fraction $\mathcal{B}(\bar{B} \rightarrow Xe^- \nu)$ was pioneered by the ARGUS collaboration.⁷ It has a small model-dependence in the sense that no assumptions on the shape of the primary electron spectrum from $\bar{B} \rightarrow Xe^- \nu$ decays are necessary. In this analysis,¹⁴ we select events by the presence of a high-momentum tag electron ($1.4 < p^* < 2.3$ GeV). In the rest of the event, signal electrons are identified and grouped into two separate classes, depending on whether they have opposite charge (“unlike sign sample”: the two electrons are either from $B \rightarrow X_{\bar{c}}e^+ \nu, \bar{B} \rightarrow X_c e^- \nu$ or from $\bar{B} \rightarrow X_c e^- \nu, X_c \rightarrow$

$Ye^+\nu$) or the same charge (“like sign sample”: $B \rightarrow X_{\bar{e}}e^+\nu, \bar{B} \rightarrow B \rightarrow X_{\bar{e}}e^+\nu$ and $B \rightarrow X_{\bar{e}}e^+\nu, \bar{B} \rightarrow X_{\bar{e}}, X_{\bar{e}} \rightarrow Ye^+\nu$) as the tag electron.

In the unlike-sign class, the background $\bar{B} \rightarrow X_e e^- \nu, X_e \rightarrow Ye^+\nu$ can be strongly reduced by exploiting the fact that electron pairs from the same B are preferentially back-to-back, while there is no correlation in the opening angle distribution $\alpha(e_{tag}, e_{signal})$ for the case of the pair coming from two different B mesons. This is illustrated in Fig. 3a, where the opening angle distribution for signal electrons with $0.7 < p^* < 0.8$ GeV shows a flat signal component and a background contribution rising toward low values. The shape information is taken from MC simulation, and the data distribution is fitted to determine the background contribution (shaded) in the signal region. The requirement of a small opening angle also removes most of the heavy pair background (from $J/\psi \rightarrow e^+e^-$; the remaining pair background from photon conversions and Dalitz $\pi^0 \rightarrow e^+e^-\gamma$ decays is reconstructed and removed explicitly). The effect of $B^0\bar{B}^0$ mixing can be unfolded, as

$$\frac{1}{\varepsilon_\alpha(p^*)} \frac{dN_{\pm\mp}}{dp^*} = \frac{dN_{primary}}{dp^*} \cdot (1 - \chi) + \frac{dN_{casc}}{dp^*} \cdot \chi \quad (3)$$

$$\frac{dN_{\pm\pm}}{dp^*} = \frac{dN_{primary}}{dp^*} \cdot \chi + \frac{dN_{casc}}{dp^*} \cdot (1 - \chi), \quad (4)$$

where $\chi = f_{00} \cdot \chi_d = 0.087$ (here $\chi_d = 0.174 \pm 0.009$ is the $B^0\bar{B}^0$ mixing parameter¹⁵ and $f_{00} = 0.50$ has been assumed) and the efficiency $\varepsilon_\alpha(p^*)$ of the opening angle requirement.

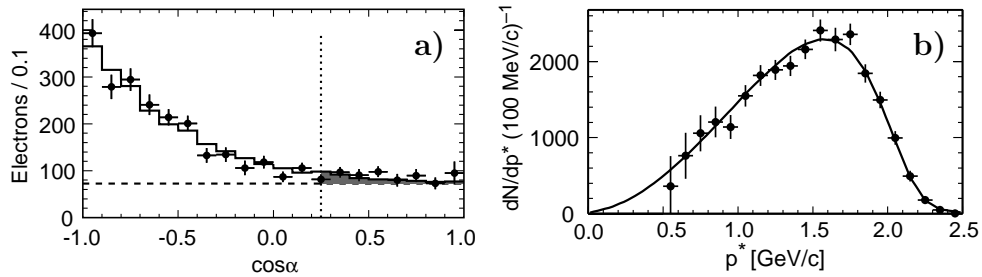


Fig. 3. a) Cosine of the opening angle between the signal electron with $0.7 < p^* < 0.8$ GeV/c and the tag electron in the unlike-sign sample. The shaded area represents the background electrons, the vertical line illustrates the minimum requirement on the opening angle. b) Momentum distribution of electrons from $\bar{B} \rightarrow Xe^- \nu$ decays, after efficiency and bremsstrahlung corrections.

The integration of the spectrum over the range $0.6 < p^* < 2.5$ GeV (see Fig. 3b) yields $N(\bar{B} \rightarrow Xe^- \nu) = 25070 \pm 410_{stat}$ signal events for an integrated luminosity of about 4 fb^{-1} . Only small corrections need to be applied: Bremsstrahlung corrections (2.2%), geometric acceptance (16%), event selection bias (2%) and the extrapolation

(6.1%) to $p^* = 0$. From these numbers and the overall normalization from the number of tag electrons we determine $\mathcal{B}(\bar{B} \rightarrow X e^- \nu) = (10.87 \pm 0.18 \pm 0.30)\%$. The dominant systematic error arise from electron identification plus tracking and from semileptonic decays of upper-vertex charm particles, especially affected by the poor knowledge of $\mathcal{B}(D_s \rightarrow \phi\pi)$. Extending the measurement range to lower values of p^* does not improve the error, as backgrounds (pair background, cascade decays) with large uncertainties grow very large.

From the total branching fraction, $|V_{cb}|$ can be extracted, *e.g.*, in the $1S$ expansion.¹⁶ The errors in this approach are dominated by theoretical uncertainties. In the next section an alternative method is described that takes into account more information and their correlations. There, the differential measurement of the lepton energy spectrum and its moments will contribute substantially.

The measurement of $\bar{B} \rightarrow X e^- \nu$ has also been done in the recoil of a B_{reco} candidate,¹⁷ albeit with much less statistics. This allows a comparison of electron energy spectra from B^0 and B^+ decays and provides one way to study effects of quark-hadron duality violation and other nonperturbative effects like weak annihilation and Pauli interference.

5.2. Hadronic Mass Moments

In $\bar{B} \rightarrow X \ell \bar{\nu}$ decays, the invariant mass m_X distribution is the most sensitive probe to physics beyond the parton model and hence to the nonperturbative parameters $\bar{\Lambda}$ and λ_1 . The lepton energy distribution also has sensitivity, but at a reduced level. The experimental feasibility matches this situation: the lepton energy distribution can be obtained with high precision and resolution from a measurement of the electron only, a relatively straightforward task. On the other hand, the reconstruction of the complete hadronic final state is a much more involved procedure.

The event selection in this analysis¹⁸ requires a B_{reco} candidate and an identified lepton with $p^* > 900 \text{ MeV}/c$ and charge consistent for a primary B decay. The charge imbalance of the event is required to be not larger than one. These criteria lead to a data sample of about 7100 events.

All remaining charged tracks and neutral showers that are not part of the B_{reco} candidate are combined into the hadronic system X . A neutrino candidate is reconstructed from the missing four-momentum $p_{miss} = p_{\mathcal{R}(4S)} - p_X - p_{B_{reco}}$, where all momenta are measured in the laboratory frame. Consistency of the measured p_{miss} with the neutrino hypothesis is enforced with the requirements $E_{miss} > 0.5 \text{ GeV}$, $|\vec{p}_{miss}| > 0.5 \text{ GeV}$, and $|E_{miss} - |\vec{p}_{miss}|| < 0.5 \text{ GeV}$. The determination of the mass of the hadronic system is improved by a kinematic fit that imposes four-momentum conservation, the equality of the masses of the two B mesons, and forces $p_\nu^2 = 0$. The resulting m_X resolution is $350 \text{ MeV}/c^2$ on average. MC simulated event samples are used to calibrate the absolute mass scale, determine efficiencies, and estimate backgrounds. This mass scale calibration allows the direct determination of the moments of the m_X distribution without recourse to simulated decay spectra.

The resulting moments of the hadronic mass-squared distribution are shown as a function of the threshold lepton momentum p_{min}^* in Fig. 4a. A substantial rise of the moments toward lower momentum is visible, due to the enhanced contributions of high-mass charm states (phase-space suppressed at higher p_{min}^*). The main contributions to the systematic error are from the detector response simulation and from semileptonic decays of upper-vertex charm particles. The uncertainty from the modeling of the X_c state is negligible compared to the other systematic errors.

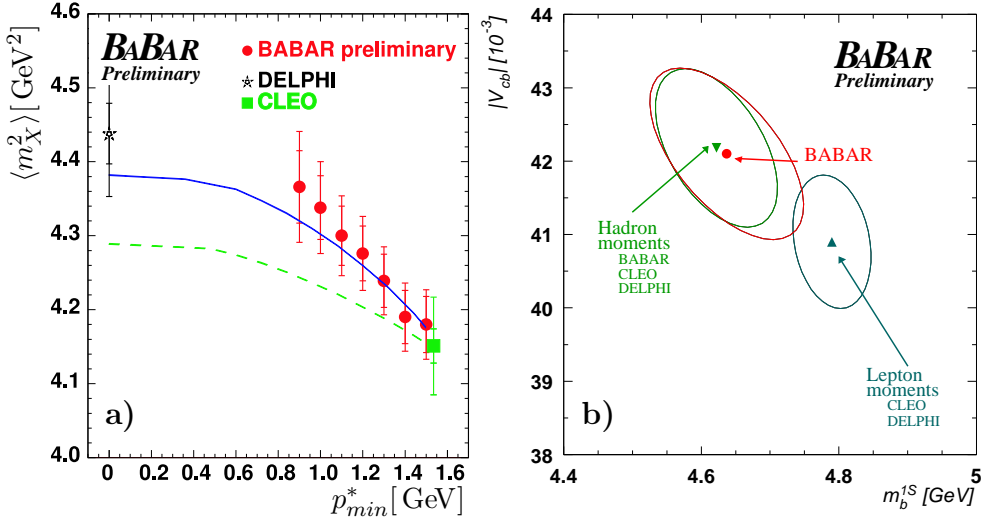


Fig. 4. (a) Measured hadronic mass moments for different lepton threshold momenta p_{min}^* . The errors of the individual *BABAR* measurements are highly correlated. For comparison, the measurements by the *DELPHI* and *CLEO* collaborations are also shown. The solid curve is a fit to the *BABAR* data; the dashed curve is the OPE prediction based on the *CLEO* result combined with information from the decay $b \rightarrow s\gamma$. (b) Constraints on the b quark mass and $|V_{cb}|$ from this measurement, and the fit to the combined hadron moments and lepton moments, respectively.

Accounting for all correlations between the moments at different p_{min}^* , we obtain $\overline{\Lambda} = 0.53 \pm 0.09 \text{ GeV}$ and $\lambda_1 = -0.36 \pm 0.09 \text{ GeV}^2$ in the $\overline{\text{MS}}$ regularization scheme.¹⁹ The errors given do not include uncertainties due to terms at $\mathcal{O}(1/m_B^3)$. For comparison, Fig. 4a also shows the result of the hadronic mass measurement of *DELPHI*,²⁰ fully consistent with this result. The *CLEO* result²¹ of the first hadronic mass moment at $p_{min}^* = 1.5 \text{ GeV}$ is also consistent, but in combination with the mean photon energy from $b \rightarrow s\gamma$ ²² shows a different p_{min}^* dependence (taking into account the bias from the limited photon energy range, the agreement is much better²³).

A fit to all hadronic moments from *BABAR* is performed in the $1S$ scheme,²⁴ as this scheme exhibits better convergence of the perturbative series than other alternatives. The results are $m_b^{1S} = 4.638 \pm 0.094_{exp} \pm 0.062_{dim\oplus BLM} \pm 0.065_{1/m_B^3} \text{ GeV}$

and $\lambda_1 = -0.26 \pm 0.06_{exp} \pm 0.04_{dim\oplus BLM} \pm 0.04_{1/m_B^3} \text{ GeV}^2$. The fit also utilizes the semileptonic width $\Gamma_{sl} = (4.37 \pm 0.18) \times 10^{-11} \text{ MeV}$ (determined from BABAR data) to determine $|V_{cb}| = (42.10 \pm 1.04_{exp} \pm 0.52_{dim\oplus BLM} \pm 0.50_{1/m_B^3}) \times 10^{-3}$.

The consistency of the OPE is tested by combining the measurement of BABAR with the four lepton energy moments measured by the CLEO collaboration²⁵ and the DELPHI collaboration.²⁰ In Fig. 4b, the fit results are shown separately for hadron mass and lepton energy moments. The $\Delta\chi^2 = 1$ contours of hadronic mass and lepton energy moments do not overlap. Note that the theoretical errors here do not include uncertainties due to terms at $\mathcal{O}(1/m_B^3)$. In the future, the extension of these measurement to include more high-precision observables will allow a quantification as to what precision can be expected realistically from the OPE.

6. Inclusive Cabibbo-suppressed Decays

In the measurement of $\bar{B} \rightarrow X_u \ell \bar{\nu}$ decays, the large background from $\bar{B} \rightarrow X_c \ell \bar{\nu}$ decays has to be reduced by restricting the phase space in the analyses. One possibility is to measure the lepton energy spectrum at the “endpoint”, beyond the kinematic cutoff for $\bar{B} \rightarrow X_c \ell \bar{\nu}$ decays, at $p^* > 2.3 \text{ GeV}$. A disadvantage of this approach is that only about 10% of all charmless semileptonic decays are measured. This leads to a significant extrapolation with corresponding uncertainties. The model-dependence of this error can be reduced with information on the movement of the b quark inside the B meson obtained from the photon energy spectrum in $b \rightarrow s\gamma$ decays.²⁶

Alternative methods have been proposed, such as the invariant mass of the hadronic system X in $\bar{B} \rightarrow X \ell \bar{\nu}$ decays.²⁷ Here 50–80% of all $\bar{B} \rightarrow X_u \ell \bar{\nu}$ decays are measured, depending which cut $m_X < m_X^{cut}$ is used for the determination of the signal yield. As in the case of the endpoint spectrum, there is a dependence on the light-cone distribution function (“shape function”) of the b quark in the B meson, describing the Fermi motion of the heavy quark in the meson. Another process sensitive to this shape function is the rare decay $b \rightarrow s\gamma$, with a branching fraction²² $\mathcal{B}(b \rightarrow s\gamma) = 3.21 \pm 0.53 \times 10^{-4}$. This rate is even smaller than $\mathcal{B}(\bar{B} \rightarrow X_u \ell \bar{\nu})$, thus limiting the precision of the determination of the shape function parametrization and parameters. If the HQET parameters determined in Cabibbo-favored semileptonic B decays can be used consistently in the shape function description, the determination of $|V_{ub}|$ will benefit from the high precision measurements described in the previous section.

The total rate can be translated to $|V_{ub}|$ with an error of about 5% from uncertainties of higher orders in the perturbative expansion and the uncertainty of the b quark mass.^{16,32}

6.1. Endpoint Spectrum

In this analysis,²⁸ the event selection is based on a high-momentum electron ($p^* > 2.0 \text{ GeV}$) and the signature of a neutrino. Specifically, we require for the

missing momentum $p_{miss} > 1 \text{ GeV}$ to be pointing into the main detector acceptance $-0.9 < \cos \theta_{miss}^* < 0.8$ and in the hemisphere opposite to the electron. At low momenta, the electron sample is dominated by electrons from $\bar{B} \rightarrow X_c \ell \bar{\nu}$ decays over a continuum background. This latter component dominates the spectrum at high momenta. We fit the continuum background with a 4^{th} degree Chebyshev polynomial in the off-resonance data and the high-momentum range in the on-resonance data. After subtraction, the signal events are visible in the range $2.3 < p^* < 2.6 \text{ GeV}$ and illustrated with the solid (red) histogram in Fig. 5b. The restriction to this momentum range yields a total of 1696 ± 133 signal events with a signal to background ratio of $S/B = 0.25$. Extending the momentum range to lower values decreases S/B due to more background from $\bar{B} \rightarrow X_c \ell \bar{\nu}$ decays, leading to substantially higher uncertainties from the modeling of $\bar{B} \rightarrow X_c \ell \bar{\nu}$ decays. On the other hand, the extrapolation is decreased, resulting in a smaller theoretical error. In the endpoint range, the partial branching fraction is determined to be $\Delta\mathcal{B}(\bar{B} \rightarrow X_u \ell \bar{\nu}) = (0.152 \pm 0.014_{stat} \pm 0.0014_{syst}) \times 10^{-3}$, where the dominant errors arise from the uncertainties in the continuum subtraction, the motion of the B meson in the $\Upsilon(4S)$ rest-frame, and the selection efficiency.

From this result, the extrapolation to the total semileptonic charmless branching fraction is done as in the CLEO analysis.²⁶ Here the shape function parameters are determined by a fit to the $b \rightarrow s\gamma$ photon energy spectrum. The result is $\mathcal{B}(\bar{B} \rightarrow X_u \ell \bar{\nu}) = (2.05 \pm 0.27_{exp} \pm 0.46_{fu}) \times 10^{-3}$, where the errors are now grouped into a first part containing the statistical and systematic uncertainty from the endpoint measurement and a second part describing the uncertainties from the extrapolation. This yields $|V_{ub}| = (4.43 \pm 0.29_{exp} \pm 0.50_{fu} \pm 0.35_{s\gamma} \pm 0.25_{\Gamma}) \times 10^{-3}$.

6.2. Hadronic Mass Spectrum

In this analysis²⁹ we use the invariant mass m_X of the hadronic system to separate $\bar{B} \rightarrow X_u \ell \bar{\nu}$ decays from the dominant $\bar{B} \rightarrow X_c \ell \bar{\nu}$ background in events tagged by the fully reconstructed hadronic decay of a B_{reco} candidate. This method offers a substantially larger signal acceptance than the endpoint measurement. The hadronic system X in the decay $\bar{B} \rightarrow X \ell \bar{\nu}$ is reconstructed from charged tracks and energy depositions in the calorimeter not associated with the B_{reco} candidate or the identified lepton. We require exactly one charged lepton with $p^* > 1 \text{ GeV}/c$, charge conservation ($Q_X + Q_\ell + Q_{B_{reco}} = 0$), and $m_{miss}^2 < 0.5 \text{ GeV}^2$. We reduce the $\bar{B}^0 \rightarrow D^{*+} \ell^- \bar{\nu}$ background with a partial reconstruction of the decay (using the π_s^+ from the $D^{*+} \rightarrow D^0 \pi_s^+$ decay and the lepton). Furthermore, we veto events with charged or neutral kaons in the recoil \bar{B} .

In order to reduce experimental systematic errors (in particular lepton identification), we determine the ratio of branching fractions R_u from N_u , the observed number of $\bar{B} \rightarrow X_u \ell \bar{\nu}$ candidates with $m_X < 1.55 \text{ GeV}/c^2$, and $N_{sl} = 29982 \pm 233$,

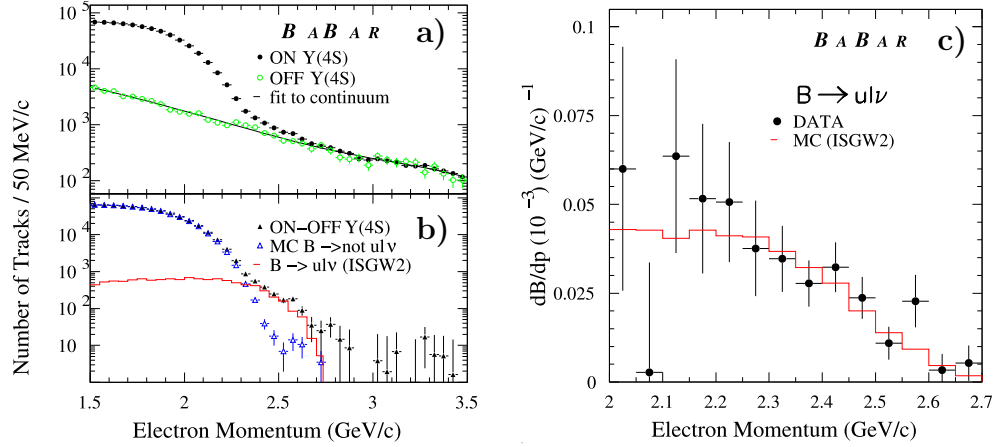


Fig. 5. a) Electron momentum distribution in the $\Upsilon(4S)$ rest-frame for on-resonance and off-resonance data, respectively. b) Electron momentum distribution after continuum subtraction, with signal and background MC distributions. c) The differential branching fraction as a function of the electron momentum, after efficiency and bremsstrahlung corrections. The data are compared to the prediction of the ISGW2 model (assuming a total inclusive branching fraction of 10^{-3} for $\bar{B} \rightarrow X_u \ell \bar{\nu}$ decays with mass $m_X < 1.5 \text{ GeV}/c^2$).

the number of events with at least one charged lepton:

$$R_u = \frac{\mathcal{B}(\bar{B} \rightarrow X_u \ell \bar{\nu})}{\mathcal{B}(\bar{B} \rightarrow X \ell \bar{\nu})} = \frac{N_u / (\varepsilon_{sel}^u \varepsilon_{m_X}^u)}{N_{sl}} \times \frac{\varepsilon_l^{sl} \varepsilon_{reco}^{sl}}{\varepsilon_l^u \varepsilon_{reco}^u}.$$

Here $\varepsilon_{sel}^u = 0.342 \pm 0.006_{stat}$ is the efficiency for selecting $\bar{B} \rightarrow X_u \ell \bar{\nu}$ decays once a $\bar{B} \rightarrow X \ell \bar{\nu}$ candidate has been identified, $\varepsilon_{m_X}^u = 0.733 \pm 0.009_{stat}$ is the fraction of signal events with the reconstructed $m_X < 1.55 \text{ GeV}/c^2$; $\varepsilon_l^{sl} / \varepsilon_l^u = 0.887 \pm 0.008_{stat}$ corrects for the difference in the efficiency of the lepton momentum cut for $\bar{B} \rightarrow X \ell \bar{\nu}$ and $\bar{B} \rightarrow X_u \ell \bar{\nu}$ decays, and $\varepsilon_{reco}^{sl} / \varepsilon_{reco}^u = 1.00 \pm 0.03_{stat}$ accounts for a possible efficiency difference in the B_{reco} reconstruction in events with $\bar{B} \rightarrow X \ell \bar{\nu}$ and $\bar{B} \rightarrow X_u \ell \bar{\nu}$ decays.

We extract N_u from the m_X distribution by a fit to the sum of three contributions: signal, background N_c from $\bar{B} \rightarrow X_c \ell \bar{\nu}$, and a background of $< 1\%$ from other sources. In each bin of the m_X distribution, the combinatorial B_{reco} background for $m_{ES} > 5.27$ is subtracted on the basis of a fit to the m_{ES} distribution. Fig. 6a shows the fitted m_X distribution. To minimize the model dependence, the first bin is extended to $m_X < 1.55 \text{ GeV}/c^2$. We find 175 ± 21 signal events and 90 ± 5 background events in the region $m_X < 1.55 \text{ GeV}$. From this we determine $R_u = (2.06 \pm 0.25_{stat} \pm 0.23_{syst} \pm 0.36_{theo}) \times 10^{-2}$. The dominant detector systematic errors are due to the uncertainty in photon detection and combinatorial background subtraction. The efficiencies ε_{sel}^u and $\varepsilon_{m_X}^u$ are sensitive to the modeling of the $\bar{B} \rightarrow X_u \ell \bar{\nu}$ decays.³⁰ We assess the theoretical uncertainties by varying the nonperturbative parameters within their errors, $\bar{\Lambda} = 0.48 \pm 0.12 \text{ GeV}$ and

$\lambda_1 = -0.30 \pm 0.11 \text{ GeV}^2$, obtained from the results in Ref. 21 by removing terms proportional to $1/m_b^3$ and α_s^2 from the relation between the measured observables and $\overline{\Lambda}$ and λ_1 . Here we assume that the parameters of the shape function are given by the HQET parameters.

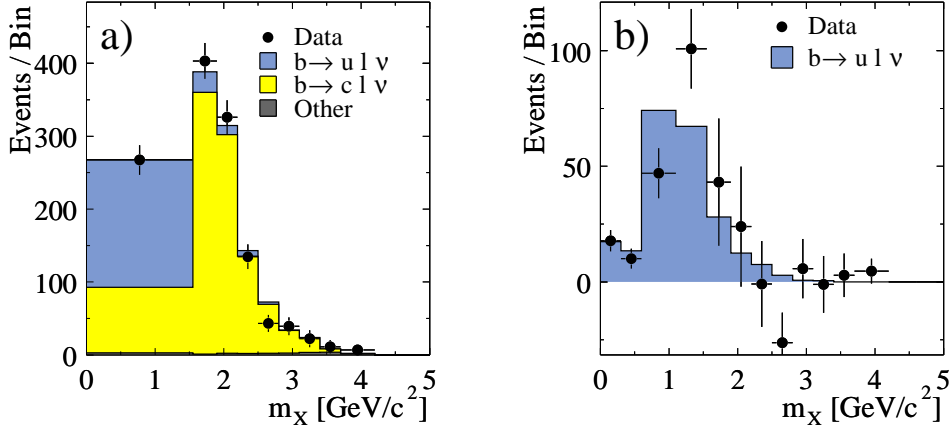


Fig. 6. The m_X distribution for $\bar{B} \rightarrow X \ell \bar{\nu}$ candidates: a) data (points) and fit components, and b) data and signal MC after subtraction of the $b \rightarrow c \ell \nu$ and the “other” backgrounds.

Combining the ratio R_u with the measured inclusive semileptonic branching fraction,¹⁴ we obtain $\mathcal{B}(\bar{B} \rightarrow X_u \ell \bar{\nu}) = (2.24 \pm 0.27 \pm 0.26 \pm 0.39) \times 10^{-3}$. With the average B lifetime³¹ we obtain $|V_{ub}| = (4.62 \pm 0.28_{stat} \pm 0.27_{syst} \pm 0.40_{theo} \pm 0.26_r) \times 10^{-3}$, where the last error is the uncertainty in the extraction of $|V_{ub}|$ from the total decay rate. No error is assigned to the assumption of parton-hadron duality. This result is consistent with previous inclusive measurements, but has a smaller systematic error, primarily due to larger acceptance and higher sample purity.

7. Exclusive Cabibbo-suppressed Decays

The reconstruction of exclusive charmless semileptonic $\bar{B} \rightarrow X_u \ell \bar{\nu}$ decays, where $X_u = \pi, \rho, \omega, \dots$, is challenging due to large backgrounds and the missing neutrino. The theoretical description is on less solid foundations than in the inclusive case. The determination of $|V_{ub}|$ in this case requires the computation of formfactors, parametrizing the behavior of the hadronic current in the B meson decay. Due to the light mass of the hadronic final state, HQET is of much less help here compared to $\bar{B} \rightarrow D^* \ell \bar{\nu}$, and most of the calculations are based on phenomenological models. Currently, lattice QCD calculations are still based on the quenched approximation, with uncertainties of the order of 15–20%. The decay $\bar{B} \rightarrow \pi \ell \bar{\nu}$ is more amenable to these calculations than the decay $\bar{B} \rightarrow \rho \ell \bar{\nu}$, where the hadronic final state is a broad resonance. The computation of formfactors is only possible in the region of

low momentum $p_\pi \leq 1$ GeV. This corresponds to high $Q^2 \geq 17$ GeV², where the rate is kinematically suppressed. In addition, this is precisely the kinematic region where the current experimental methods are limited by very high backgrounds. With the high luminosities achievable at the B factories, the measurement of exclusive decays in the recoil of a B_{reco} candidate offers large advantages.

7.1. $B^0 \rightarrow \rho^- e^+ \bar{\nu}$

This analysis³³ aims for a high neutrino reconstruction efficiency and is similar to a previous CLEO analysis.³⁴ Events are selected with a high-momentum electron and divided into two samples based on the electron momentum: The high-momentum *high- E_e* with $2.3 < E_e < 2.7$ GeV and *low- E_e* $2.0 < E_e < 2.3$ GeV. The *high- E_e* sample is primarily used for the determination of the signal, while the *low- E_e* sample serves for the measurement of the $\bar{B} \rightarrow X_c \ell \bar{\nu}$ background. The analysis is optimized for the measurement of $B \rightarrow \rho e^+ \nu$, but also selects $B \rightarrow \pi e^+ \nu$ and $B^+ \rightarrow \omega e^+ \nu$ to better control cross-feed background contributions.

Continuum background is suppressed with a neural network of 14 variables. As the hadronic final state in this exclusive analysis is much less constrained than in $\bar{B} \rightarrow D^* \ell \bar{\nu}$, the neutrino reconstruction carries more weight. The direction of the missing momentum is required to point into the main detector ($|\cos \theta_{miss}| < 0.9$) to reject events with substantial energy loss along the beam axis. The angle α between the reconstructed missing momentum and the inferred neutrino momentum is required to be small ($\cos \alpha > 0.8$) and (as in the decay $\bar{B} \rightarrow D^* \ell \bar{\nu}$) the angle between the B meson momentum and the combined eh momentum (where $h = \pi, \rho, \omega$) is required to lie in the physical region ($|\cos \theta_{B,eh}| < 1.1$).

The signal yield is extracted by a binned maximum likelihood fit to *high- E_e* and *low- E_e* samples in two variables: $\Delta E^* = E_{had} + E_e + p_{\bar{\nu}} - E_{beam}$ (where $p_{\bar{\nu}}$ is obtained from the missing momentum) and the mass of the hadronic system $m_{had} = m_{\pi\pi(\pi)}$. The shape of the continuum distributions is taken from off-peak data, the remaining shapes are from MC simulations. The fit incorporates isospin and quark model relations. Fig. 7a illustrates the $m_{\pi\pi}$ variable in the *high- E_e* sample. For an integrated luminosity of $\mathcal{L} = 50 \text{ fb}^{-1}$, a signal yield of $S = 505 \pm 63_{stat}$ events is obtained, leading to a branching fraction of $\mathcal{B}(B^0 \rightarrow \rho^- e^+ \bar{\nu}) = (3.29 \pm 0.42_{stat} \pm 0.47_{syst} \pm 0.60_{theo}) \times 10^{-4}$. The CKM matrix element $|V_{ub}|$ is determined from the relation $|V_{ub}| = \sqrt{\frac{\mathcal{B}(B^0 \rightarrow \rho^- e^+ \bar{\nu})}{\Gamma_{theo} \tau_{B^0}}} = (3.64 \pm 0.22_{stat} \pm 0.25_{syst}^{+0.39}_{-0.56_{theo}}) \times 10^{-3}$. The dominating systematic error are from the modeling of resonant and nonresonant $\bar{B} \rightarrow X_u \ell \bar{\nu}$ decays, the tracking efficiency, and the fit method. The theoretical error is determined as half of the full spread of all theoretical uncertainties in the formfactor calculations.³⁵ A measurement of the Q^2 dependence will help to reject models not describing $\bar{B} \rightarrow \rho e \bar{\nu}$ decays, but will not help in reducing the inherent model dependence of the error. Here, only unquenched lattice QCD calculation of the formfactors and the experimental measurement in the same kinematic region will advance the field.

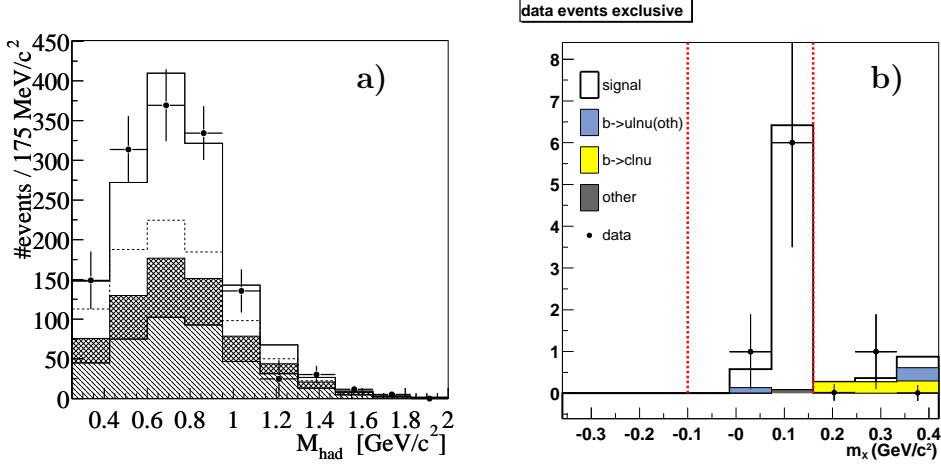


Fig. 7. Illustration of the signal to background ratio for exclusive charmless semileptonic decays. a) Continuum-subtracted fit projections for $m_{\pi^0\pi^-}$ for the $B^0 \rightarrow \rho^- e^+ \nu$ channel in the *high- E_e* electron-energy region. The contributions are the direct and crossfeed components of the signal (unhatched region, above and below the dashed line, respectively), the background from $b \rightarrow ue\nu$ (double-hatched region), and $b \rightarrow ce\nu$ and other backgrounds (single-hatched region). b) The m_X projection for $B^- \rightarrow \pi^0 \ell^- \bar{\nu}$ measured on the recoil of a fully reconstructed hadronic B decay.

7.2. Exclusive Decays on the Recoil

This analysis³⁶ is a combination of the high-purity event tagging based on a fully reconstructed hadronic B decay and the exclusive reconstruction of signal decay in the recoil. This approach results in a very low overall signal efficiency of the order of 0.1%, but allows the measurement of $\bar{B} \rightarrow \pi \ell \bar{\nu}$ over the entire kinematic range. This type of measurement will become a prime method for the determination of $|V_{ub}|$ from exclusive semileptonic decays, as the traditional approach mentioned in the previous section is affected by very low S/B problems, especially in the range where lattice QCD can provide model-independent formfactor calculations. Because the statistical yield of the method is low, an integrated luminosity of about $\mathcal{L} \sim 500 \text{ fb}^{-1}$ is needed before the method will provide a better measurement of $\bar{B} \rightarrow \pi \ell \bar{\nu}$ than the traditional approach.

While all exclusive decays can be measured in this analysis paradigm, only the measurement $\bar{B} \rightarrow \pi \ell \bar{\nu}$ shall be described here (for $B^- \rightarrow \pi^0 \ell^- \bar{\nu}$) as it is the most promising channel for lattice QCD calculations. After the requirement of a fully reconstructed hadronic B decay for tagging purposes, events with semileptonic B decays are selected by the requirement of a muon or electron with $p_\ell > 1.0 \text{ GeV}$. Cabibbo-favored $\bar{B} \rightarrow X_c \ell \bar{\nu}$ decays are rejected by requirements on the missing mass $m_{\text{miss}}^2 < 0.4 \text{ GeV}^2$, the invariant mass of the π^0 candidate and the requirement that no other hadronic charged track be detected. The number of signal $S = 7.0 \pm 2.6$ events is determined from a fit to the m_{ES} distribution of selected events, corrected for background $B = 0.2 \pm 0.2$ (determined

from MC simulations) and selection efficiency $\varepsilon = 0.42 \pm 0.04$ for all requirements after the B_{reco} and lepton candidate selections. As in the case of the inclusive $\bar{B} \rightarrow X_u \ell \bar{\nu}$ analysis, the signal yield is normalized to the number of events with a charged lepton in the recoil of the B_{reco} candidate. The result of this analysis yields $\mathcal{B}(B^- \rightarrow \pi^0 \ell^- \bar{\nu})/\mathcal{B}(\bar{B} \rightarrow X \ell \bar{\nu}) = (0.76 \pm 0.31_{stat} \pm 0.11_{syst}) \times 10^{-3}$. This result is statistics limited; the largest systematic errors are uncertainties of the m_{ES} fits, a possible selection bias for charmless semileptonic B decays compared to general semileptonic B decays, and the measurement of photons in the calorimeter.

8. Conclusions

In the last few years, the study of semileptonic B decays has offered many new perspectives. Theoretical uncertainties are parametrized in terms of experimental observables, substantially reducing the model-dependent component in the total error on $|V_{cb}|$. The large luminosity at experiments like BABAR at the $\Upsilon(4S)$ resonance allows to select events by means of fully reconstructed hadronic B decays and studying the semileptonic decay of the other B meson. This opens the precise study of spectral moments in semileptonic B decays and therefore the precision determination of $|V_{cb}|$ and the underlying fundamental parameters of the theory. It also allows for better constraints in the study of $\bar{B} \rightarrow X_u \ell \bar{\nu}$ decays and leads to improved determinations of $|V_{ub}|$. In the future, the measurement of exclusive charmless semileptonic B decays in combination with unquenched lattice QCD calculations will challenge the precision of inclusive $|V_{ub}|$ determinations. In the far future, leptonic B decays may provide yet another way to $|V_{ub}|$.

9. Acknowledgements

It is a pleasure to acknowledge the collaboration with O. Buchmüller, D. del Re, R. Faccini, E. Hill, V. Lüth, and A. Sarti. I have enjoyed instructive discussions with C. Bauer, T. G. Becher, Z. Ligeti, and N. Uraltsev.

1. Z. Ligeti, arXiv:hep-ph/0309219.
2. M. Luke, eConf **C0304052**, WG107 (2003) arXiv:hep-ph/0307378.
3. For recent introductions, see, *e.g.*, Z. Ligeti, eConf **C020805**, L02 (2002) arXiv:hep-ph/0302031; G. Buchalla, arXiv:hep-ph/0202092; N. Uraltsev, arXiv:hep-ph/9804275.
4. E. Eichten and B. Hill, Phys. Lett. B **234**, 511(1990); Phys. Lett. B **243**, 427(1990); H. Georgi, Phys. Lett. B **240**, 447(1990); M. Neubert, Phys. Rep. B **245**, 259(1994).
5. J. Chay, H. Georgi and B. Grinstein, Phys. Lett. B **247**, 399 (1990); I. I. Bigi, N. G. Uraltsev and A. I. Vainshtein, Phys. Lett. B **293**, 430 (1992) [Erratum-ibid. B **297**, 477 (1993)]; I. I. Bigi, B. Blok, M. A. Shifman, N. G. Uraltsev and A. I. Vainshtein, arXiv:hep-ph/9212227; I. I. Bigi, M. A. Shifman, N. G. Uraltsev and A. I. Vainshtein, Phys. Rev. Lett. **71**, 496 (1993); A. V. Manohar and M. B. Wise, Phys. Rev. D **49**, 1310 (1994); B. Blok, L. Koyrakh, M. A. Shifman and A. I. Vainshtein, Phys. Rev. D **49**, 3356 (1994) [Erratum-ibid. D **50**, 3572 (1994)].
6. B. Aubert *et al.* [BABAR Collaboration], Nucl. Instrum. Meth. A **479**, 1 (2002).

7. H. Albrecht *et al.* [ARGUS Collaboration], Phys. Lett. B **318**, 397 (1993);
8. N. Isgur and M. B. Wise, Phys. Lett. B **232**, 113 (1989); N. Isgur and M. B. Wise, Phys. Lett. B **237**, 527 (1990).
9. M. E. Luke, Phys. Lett. B **252**, 447 (1990).
10. B. Aubert *et al.* [BABAR Collaboration], arXiv:hep-ex/0308027.
11. C. G. Boyd, B. Grinstein and R. F. Lebed, Phys. Rev. D **56**, 6895 (1997); I. Caprini, L. Lellouch and M. Neubert, Nucl. Phys. B **530**, 153 (1998).
12. S. Hashimoto, A. S. Kronfeld, P. B. Mackenzie, S. M. Ryan and J. N. Simone, Phys. Rev. D **66**, 014503 (2002).
13. R. A. Briere *et al.* [CLEO Collaboration], Phys. Rev. Lett. **89**, 081803 (2002).
14. B. Aubert *et al.* [BABAR Collaboration], Phys. Rev. D **67**, 031101 (2003).
15. D. E. Groom *et al.* [PDG Collaboration], Eur. Phys. J. C **15** (2000) 1.
16. A. H. Hoang, Z. Ligeti and A. V. Manohar, Phys. Rev. Lett. **82**, 277 (1999).
17. U. Langenegger [for the BABAR Collaboration], arXiv:hep-ex/0204001.
18. B. Aubert *et al.* [BABAR Collaboration], arXiv:hep-ex/0307046.
19. A. F. Falk and M. E. Luke, Phys. Rev. D **57**, 424 (1998).
20. M. Calvi [for the DELPHI Collaboration], arXiv:hep-ex/0210046.
21. D. Cronin-Hennessy *et al.* [CLEO Collaboration], Phys. Rev. Lett. **87**, 251808 (2001).
22. S. Chen *et al.* [CLEO Collaboration], Phys. Rev. Lett. **87**, 251807 (2001).
23. I. I. Bigi and N. Uraltsev, Phys. Lett. B **579**, 340 (2004).
24. C. W. Bauer, Z. Ligeti, M. Luke and A. V. Manohar, Phys. Rev. D **67**, 054012 (2003).
25. R. A. Briere *et al.* [CLEO Collaboration], arXiv:hep-ex/0209024.
26. A. Bornheim *et al.* [CLEO Collaboration], Phys. Rev. Lett. **88**, 231803 (2002).
27. V. D. Barger, C. S. Kim, and R. J. Phillips, Phys. Lett. B **251**, 629 (1990); A. F. Falk, Z. Ligeti, and M. B. Wise, Phys. Lett. B **406**, 225 (1997); I. I. Bigi, R. D. Dikeman, and N. Uraltsev, Eur. Phys. J. C **4**, 453 (1998).
28. B. Aubert *et al.* [BABAR Collaboration], arXiv:hep-ex/0207081.
29. B. Aubert *et al.* [BABAR Collaboration], arXiv:hep-ex/0307062.
30. F. De Fazio and M. Neubert, JHEP **9906**, 017 (1999).
31. K. Hagiwara *et al.* [PDG Collaboration], Phys. Rev. D **66**, 010001 (2002).
32. N. Uraltsev, Int. J. Mod. Phys. A **14**, 4641 (1999).
33. B. Aubert *et al.* [BABAR Collaboration], Phys. Rev. Lett. **90**, 181801 (2003).
34. B. H. Behrens *et al.* [CLEO Collaboration], Phys. Rev. D **61**, 052001 (2000).
35. D. Scora and N. Isgur, Phys. Rev. D **52**, 2783 (1995); M. Beyer and D. Melikhov, Phys. Lett. B **436**, 344 (1998); L. Del Debbio, *et al.* [UKQCD Collaboration], Phys. Lett. B **416**, 392 (1998); P. Ball and V. M. Braun, Phys. Rev. D **58**, 094016 (1998); Z. Ligeti and M. B. Wise, Phys. Rev. D **53**, 4937 (1996).
36. D. del Re [for the BABAR collaboration], “Measurements of Semileptonic B Decays with BABAR”, Poster shown at Lepton-Photon 2003.